Optical Materials 133 (2022) 113019

Contents lists available at ScienceDirect

Optical Materials

journal homepage: www.elsevier.com/locate/optmat

Research Article

Anti-reflective and superamphiphilic coatings on polycarbonate

P.T. Valentim [a], A. Retolaza [a], J. Llobet [b], C. Araújo [c], S. Cruz [c], C. Machado [d], A.J.V. Pontes [d], H. Santos [e], P.C. Sousa [a,*]

[a] INL – International Iberian Nanotechnology Laboratory, Av. Mestre José Veiga, 4715-330, Braga, Portugal
[b] IMB-CNM CSIC - Institut de Microelectrònica de Barcelona, Campus UAB, 08193 Bellaterra, Catalonia, Spain
[c] PIEP – Center for Innovation in Polymer Engineering, University of Minho, 4800 Guimarães, Portugal
[d] IPC – Institute of Polymers and Composites, Department of Polymer Engineering, University of Minho, 4800-058, Guimarães, Portugal
[e] InovePlastika, S.A, 4755-521, Barcelos, Portugal

ARTICLE INFO

Keywords:
Transmission
Polycarbonate
Polymer
Transfer matrix method
Amphiphilic coatings

ABSTRACT

In this work, we investigated the transmission enhancement of a polycarbonate substrate (PC) at the beginning of the near-infrared part of the electromagnetic spectrum, by incorporating anti-reflective coatings (ARC) on the surface. Thin film ARC formed by combining layers of SiO_2, TiO_2, and SiNx were studied, and the influence of the layers thickness on the optical response of the systems was explored, with the objective of keeping the fabrication process simple, while maintaining high levels of light transmission. Moreover, we compare the results obtained with the thin film ARC with those for a more complex system formed by a hexagonal array of nanopillars. Transmission values close to 100% were theoretically predicted for both systems and experimentally measured with the thin film ARC. Additionally, we report a superamphiphilic behaviour for the thin film ARC studied experimentally, after contact angle measurements, which renders self-cleaning properties to the surface of the systems.

1. Introduction

Glass has been extensively used as the main material to fabricate optical components due to its mechanical properties, chemical inertness, thermal stability, and excellent optical transparency [1]. Although, new manufacturing routes have been shaped for using polymers with improved flexibility, high precision, and reduced weight of the final products. Polymers can be found more suitable for many industrial applications because they can reproduce or even overcome glass properties, and have the potential to reduce manufacturing costs. Furthermore, polymer substrates in which optical reflection is suppressed from the surface are essential for a broad range of applications, such as displays, windshields, photovoltaic cells, and light detector systems, as for example light detection and ranging (LiDAR) systems, to cite a few [2–4].

The demand for more sensitive, selective, and robust detectors pushes the natural optical transmittance levels of the materials to the limit. In order to further increase the transmittance of light, while reducing reflectance to a minimum, different strategies have been employed. These strategies rely on depositing thin film ARC on the surface of the material, as well as modifying their surface roughness by creating micro and nano-structures or generating nano-particles on the surface [5]. Thin film ARC are made of single-layer or multi-layer films with different refractive indices (RI), which reduces the reflection due to the destructive interference of the multiple wavefronts reflected at each interface [6,7]. The optimization of an ARC for a specific spectral region depends on the number, thicknesses, and optical properties of the selected materials, as well as on the type of substrate to be used.

Multilayer ARC have been applied to glass optics for decades [5,8], with TiO_2 and SiO_2 being the most used materials, which are typically stacked in a layered structure with other materials such as ZnO, WO_3, Cr_2O_3, VO_3, Al_2O_3, and MgF_2 [9]. On the other hand, studies that describe ARC on polymer substrates report that these systems may present thermal limitations, due to the low vitric point of the substrates, and that they also can interact with plasma which can lead to adhesion modifications [8]. Additionally, the transmission enhancement caused by quarter-wave coatings in the index-matching approach presents a theoretic limit imposed by the materials involved in the system. Increasing the number of layers and using different materials can overcome these difficulties, however, raising the costs of fabrication

* Corresponding author.
E-mail address: patricia.sousa@inl.int (P.C. Sousa).

https://doi.org/10.1016/j.optmat.2022.113019
Received 13 July 2022; Received in revised form 12 September 2022; Accepted 15 September 2022
Available online 1 October 2022

[10].

Another approach for transparent ARC inspired by nature is the biomimetic moth-eye based on the presence of nanostructures on the surface [4,6]. This approach is efficient in order to reduce the reflection of light because a smooth RI gradient is created between the air and interface and, at the same time, self-cleaning properties are created on the surface [11]. Self-cleaning properties are of particular interest for coatings employed in outdoor areas or when it is necessary to remove contaminants, such as dust or microorganisms.

In this work, we studied the enhancement of light transmission, at the beginning of near-infrared (NIR), through a PC substrate that can potentially be used to fabricate lenses for LiDAR systems. In one approach, the ARC are formed by thin layers of three different dielectric materials, namely SiO_2, TiO_2, and SiNx. Different arrangements of these thin films are used to generate a single layer and a double layer ARC on the surfaces of the polymer. We intended to increase the transmittance of light at the beginning of the NIR, with the central wavelength being at 905 nm. First, we simulated numerically the optical structures, then we manufactured them, and finally, we measured their optical response. The study was performed in order to be easily scalable to the industry. Additionally, we also studied numerically the effects of modifying the upper surface of the PC substrate by introducing a hexagonal array of nanopillars (NP) on the transmission response of the system. The theoretical results obtained with the NP were compared to those observed with the thin film ARC systems.

2. Methods

2.1. Optical calculations

The reflectance and transmittance intensities of the ARC systems under investigation were calculated using the open-source software, OpenFilters, developed by Larouche and Martinu [12]. The software uses the matrix method to calculate R and T. Here, no needle or other optimization algorithms were used. In the calculations, we considered substrates 2 mm thick and the thicknesses of the coatings were varied around $\lambda/4$ for each system. The central wavelength (λ_0) was 905 nm. The surrounding environment was air, with RI (n) and coefficient of extinction (k) being 1 and 0, respectively. Three different configurations were considered for thin film systems, which are illustrated in Fig. 1. They consist of: a single layer of SiO_2 on both faces (ARC_1); a double layer of TiO_2+SiO_2 on the front and a single layer of SiO_2 on the back (ARC_2); and a double layer of SiNx + SiO_2 on the front and back of the polymer surfaces (ARC_3).

The asymptotic values of n for the materials used in the different layers are shown in Table 1. These values, employed in the numerical calculations, were obtained experimentally from ellipsometric measurements using the test samples described in Section 3.2. Once again, the corresponding values of k were negligible. The system was illuminated by a non-polarized white light source, CIE-D65, at normal incidence angle, and the transmission signal was collected at the same angle by a detector, CIE-1931, within the range of 200 nm–1200 nm.

Table 1
RI of the polymer and coatings used.

	PC	TiO_2	SiO_2	SiNx
n	1.65	2.14	1.41	2.03

For the system composed of NP on the surface of the polymer substrate, the transmission intensities were obtained using a 3D Finite-Difference Time-Domain (FDTD) method using the software Ansys Lumerical. The structure consisted of a hexagonal array of PC NP, with height (H), radius (r), and pitch (a) on the top of a 2 mm thick PC substrate. The simulations were done considering one unit cell of the NP array. Moreover, the mesh size was of 10 nm along the xyz axes, defined after convergence tests. A simulation time of 200 fs, a planar wave source and a power detector within the range of 500 nm–1000 nm were used, and 200 data points were collected. The RI data of the PC measured experimentally (section 2.3) was used in the simulations and fitted by the software with a standard RMS error of 0.0015.

2.2. Experimental tests

PC substrates (LupizetaTM EP5000 from Mitsubishi), shaped in the form of 2 mm thick flat discs and 5 cm in diameter, were fabricated by injection molding and used to accommodate the thin film ARC. With the objective of enhancing the transmission of the light through the PC substrate, while maintaining the fabrication process simple, we experimentally studied the same 3 optical systems investigated in the numerical simulations, which are illustrated in Fig. 1.

For all coating depositions, the PC substrates were mounted on support silicon wafers. Both SiO_2 and SiNx were deposited using a plasma enhanced chemical vapor deposition (PECVD) system (SPTS), whereas the TiO_2 layer was deposited using an RF magnetron confocal sputtering system (KS1000, Kenosistec).

The PECVD tool employed is typically used for depositing a multitude of thin films on silicon substrates at 300 °C, but in this work, we decreased the operating temperature of the tool to 100 °C, which is below the glass transition temperature of the polymer used. The system has a duality of RF operation modes, and the deposition of the SiO_2 was performed using high frequency (HF) at 13.56 MHz and 30 W, whereas SiNx was deposited in low frequency (LH) at 380 kHz and 60 W. The deposition of the SiO_2 occurs at 900 mTorr and the flow rates of the used gases are: 1420 sccm of N_2O, 392 sccm of N_2, and 10 sccm of SiH_4. For the deposition of the SiNx, the base pressure is 550 mTorr and flow rates of the gases are: 40 sccm of SiH_4; 20 sccm of NH_3 and 1960 sccm of N_2.

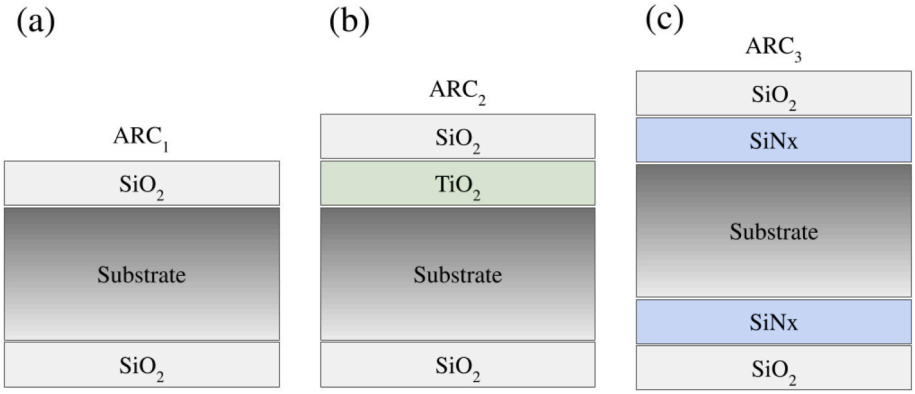

Fig. 1. Schematics of the three different optical systems investigated: (a) ARC_1 – a single layer of SiO_2 on both faces of the polymer; (b) ARC_2 – a double layer of TiO_2+SiO_2 on the front polymer surface and a single layer of SiO_2 on the back; (c) ARC_3 – a double layer of SiNx + SiO_2 on the front and back polymer surfaces.

Prior to the deposition on the polymer substrates, we calibrated the deposition rate using silicon substrates and measured the film thicknesses using interferometry (OPM/Nanocalc UV-NIS, Ocean Optics).

The sputtering deposition of the TiO_2 layer was carried out at room temperature (~ 21 °C), with the vacuum chamber being pumped down to a base pressure of 6×10^{-7} mbar and the process performed at a power of 60 W, using a high purity 2-inch diameter target of TiO_2 (purity of 99.99%, provided by Testbourne) in an argon plasma at a pressure of 1.4×10^{-2} mbar. The flow rate of argon was kept constant at 20 sccm. The distance between the substrate and the sputtering target was 20 cm and the substrate was rotating at 10 rpm.

2.3. Characterization of the ARC

The experimental test samples were characterized using an ellipsometer (model M−2000, J. A. Woollam) in the range of wavelengths from 375 nm to 998 nm. The polarization-related parameters, Δ and φ, obtained from the ellipsometric experiments were adjusted using the software of the manufacturer, named CompleteEase. The generated dispersion curves were modelled applying the Cauchy formula parametrized by the B-spline model.

Transmittance experiments were done using a UV-VIS-NIR spectrophotometer (Lambda 950 from PerkinElmer), firstly on the bare substrates, and after on the samples with the ARC. All measurements were performed within the range of 250 nm–1000 nm in steps of 5 nm. The UV-VIS part of the spectrum was detected using a photomultiplier detector with an accumulation time of 0.2 s and automatic gain. The NIR part was detected by an InGaAs detector with an accumulation time of 1 s and a gain of 15.

Static contact angle measurements were carried out using a drop shape analysis system (DSA-100, Krüss GmbH). For that, 5 μl droplets of deionized water and sunflower oil were deposited on the surface of the test samples and images were immediately recorded. Measurements were done at a controlled temperature (21 °C) and relative humidity of 45%.

For the morphological characterization of the different layers of the ARC samples and their thickness, we used the Scanning Electron Microscope/Focused Ion Beam (SEM/FIB) Cross-beam 550 (Carl Zeiss). We first deposited a thin and rough layer of Au (5–10 nm) by sputtering (Bio Rad E−5000 Polar Division). This step is to ensure a smooth cross-section, preserving the integrity of the different layers, avoiding charging effects due to the insulating nature of the inspected materials. After this preliminary step, it is programed FIB milling processes to produce fresh slides of the different samples for SEM inspection. We used an ion beam of gallium at 50 pA and 30 kV to perform the FIB cuts. The sample is positioned at 54° to have the ion beam perpendicular to the surface of the sample and the SEM column at 36° for real time inspection. The SEM conditions were low voltage (3 keV) and small current (100 pA) to reduce charging. The images can be seen in Fig. 2.

After the depositions, measurements done by contact profilometry, ellipsometry, and FIB/SEM returned an average thickness of 80 nm for TiO_2, 80 nm for SiNx, and 180 nm for SiO_2.

3. Results and discussion

3.1. Surface wettability

Static contact angles of water (WCA) and oil (OCA) were measured before and after the fabrication of the three ARC studied. In Fig. 3 and Fig. 4 we present the images acquired for the static contact angles measurements using drops of water and oil, respectively.

The results obtained from the WCA measurements confirm that the polymeric substrate presents a quasi-hydrophobic behaviour, since the WCA is close to 90° (Fig. 3a). Although, when any of the three ARC was deposited on the polymer surface, the wettability of the surface changes drastically and it is no longer possible to measure the water contact angle (WCA≈0), rendering superhydrophilic characteristics to the surface (Fig. 3b–d). Note that a superhydrophilic surface, which is characterized by contact angles below 5°, spreads water droplets to form a film throughout itself, allowing the light waves to pass through [13] and, at the same time, rendering self-cleaning properties to the surface, which from the point of view of LiDAR detectors is very advantageous. Similarly, the three ARC investigated also revealed superoleophilic behaviour with OCA below 5° as observed in Fig. 4. Such surfaces that enable the total spreading of water and oil droplets are defined as superamphiphilic surfaces and have a great potential for different applications. They are attractive for anti-fogging, self-cleaning and anti-fouling coatings, because oily contaminants can easily be removed by a stream of water [14,15], and have particular potential for inhibiting the adhesion of microorganisms in liquid media. Inspired in the leaf of Ruellia devosiana, a plant that exists in nature with amphiphilic properties, various studies have investigated artificial surfaces with similar properties. Examples rely on coatings based on TiO_2 [16] and mesoporous SiO_2 [17]. Nevertheless, the production of a superamphiphilic coating still remains a challenge. It is worth mentioning that the amphiphilic properties of the coatings developed in this work remained unchangeable for one year of experimental testing, conferring long-lasting amphiphilic properties.

3.2. Effect of coating thickness

The experimental deposition of ARC layers with precise thicknesses relies on many parameters, being sometimes challenging to control. For this reason, it is important to study systems that show reasonably high transmission levels even when deviations in the final deposited layers are observed. We investigated numerically the role played by varying the thickness of the ARC layers and the effect of that on the optical response of each system. The transmission values of the ARC with different thicknesses were compared to those calculated considering $\lambda/4$ layers.

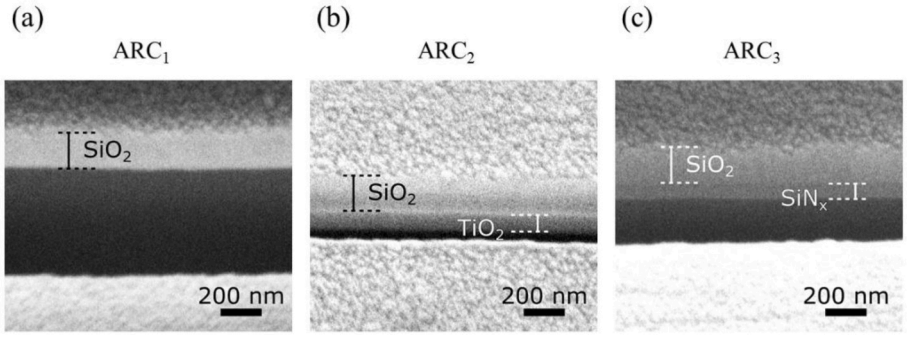

Fig. 2. Cross-section SEM/FIB images of the front faces of the ARC. (a) SiO_2 on the top of the PC substrate, ARC_1. (b) $TiO_2 + SiO_2$ on the top of PC substrate, ARC_2. (c) SiNx + SiO_2 on the top of PC substrate, ARC_3.

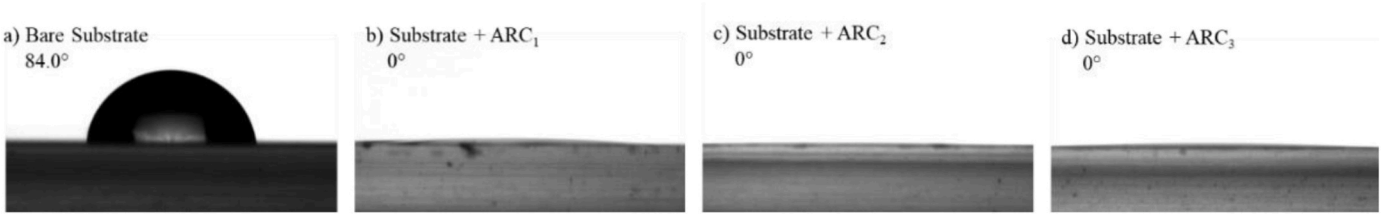

Fig. 3. Images of WCA on the surface of the: (a) bare substrate; (b) thin film of SiO_2 (ARC_1); (c) thin film of TiO_2+SiO_2 (ARC_2); and (d) thin film of SiNx + SiO_2 (ARC_3).

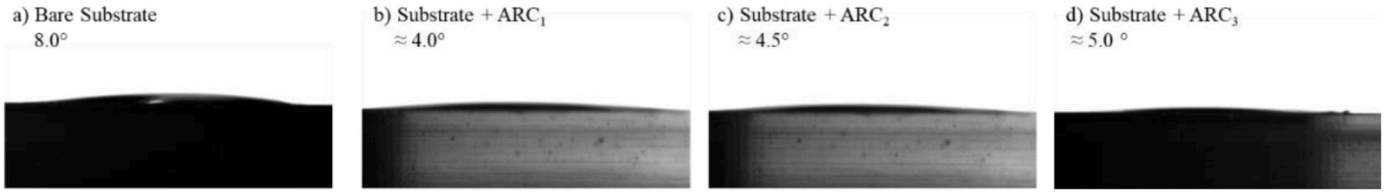

Fig. 4. Images of OCA on the surface of the: (a) bare substrate; (b) thin film of SiO_2 (ARC_1); (c) thin film of TiO_2+SiO_2 (ARC_2); and (d) thin film of SiNx + SiO_2 (ARC_3).

For the case of the ARC_1 the theoretical maximum transmittance corresponds to a SiO_2 $\lambda/4$ layer of 160 nm. In order to understand the effect of varying the layer thickness on the light transmittance, we varied concomitantly the thickness of the front and back SiO_2 layers from 100 nm to 220 nm. Fig. 5 shows a transmission intensity map as a function of the front and back layer thickness (L).

It is noticeable from Fig. 5 that the maximum transmission intensity changes with the thickness of the layers, as previously observed by Sayed et al. [18] in ARC systems of silicon oxynitride (SiON) and SiO_2 on silicon substrates. Thinner layers move the transmission intensities towards the small wavelengths, and on the other hand, thicker layers move them towards the higher wavelengths. Using a monolayer of 260 nm of SiO_2 deposited by sol-gel on the top of glass substrates, Yadav and Kim [19] have observed transmission of 95% in relation to the 90% of the bare substrate in the visible range of the spectrum. In our case, at the λ_0, it is observed 98.3% of transmission for the layer $L_{\lambda/4} = 160$ nm.

Fig. 6a shows the transmission spectra for the same optical system composed of the substrate and ARC_1 with different thicknesses. The absolute difference (Δ) between the transmission of an optical system with a $\lambda/4$ layer ($T_{\lambda/4}$) and other thicknesses (T_L) is shown in Fig. 6b for the central wavelength.

It is interesting to note that a variation in the thickness of the ARC of ±20 nm, corresponding to ±12.5% of the ideal optical one-quarter wavelength in relation to the layers L_3 and L_5, leads to a small deviation of 0.005 in the transmission of light. In practical terms, deposition rates can vary between processes, due to the variations in a parameter such as pressure, temperature, power, or bias voltage. However, these results show a relatively large tolerance in the transmission intensity regarding the variation of thicknesses of the layers. Similar observations were reported by Matsuoka et al. [20] concerning ARC for mid-infrared systems, formed by depositions of very thin films of zinc sulphide (ZnS), yttrium fluoride (YF_3) and germanium (Ge) on indium phosphate (InP) substrates. The authors theoretically show that including 5% of random variations in the thickness of the films generated less than 1.5% of changes in the reflection of the systems.

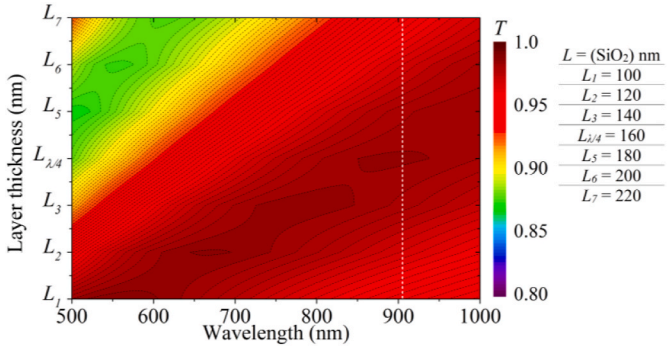

Fig. 5. Transmission intensity map as a function of the thicknesses of the SiO_2 layers. The dashed line shows the position of $\lambda_0 = 905$ nm on the map.

Additionally, we studied the optical system composed of the polymer substrate and the ARC_2 and the transmission spectra were accessed. $TiO_2 + SiO_2$ coatings are largely used in photovoltaic systems to increase the transmission and thus the power generation capacity. For instance, Zambrano et al. [21] fabricated a broadband ARC formed by two double layers of TiO_2 + SiO_2 deposited on a glass substrate solar cell. They obtained approximately 100% of transmission in the range between 550 nm and 750 nm using combinations of $\lambda/4$ and $\lambda/2$ layers. In our case, the $\lambda/4$ thicknesses of the TiO_2 and SiO_2 layers were 105 nm and 160 nm ($L_{\lambda/4}$), respectively. The calculations were done following the same protocol used for the ARC_1 system. Fig. 7 shows an intensity map of the transmission as a function of the thickness of the layers. In this case, the TiO_2 thickness varied from 20 nm to 120 nm (front face) and the SiO_2 from 120 nm to 220 nm (both faces), both in steps of 20 nm. At λ_0 the highest transmission values are observed for the layers L_3, $L_{\lambda/4}$ e L_5, with intensities of 97.2%, 96.5%, and 96.9%, respectively.

Fig. 8a compares the transmission spectra obtained for the bare substrate with those obtained for the substrate and the ARC_2 with different thicknesses. At the central wavelength, it is observed the gain on transmission levels for almost all thicknesses of ARC_2, except for the thickest, L_7.

The results in Fig. 8 reveal that the transmissions at λ_0 for L_3 and L_5 layers are very close to that for $\lambda/4$. This can be seen in more detail in Fig. 8b, where the absolute intensity variation of L with respect to$\lambda/4$ as a function of the thickness is plotted. As can be observed, Δ is practically negligible for thicknesses L_3 and L_5 in relation to$\lambda/4$.

Similarly, we performed the same analysis for the ARC_3 system. In Fig. 9 we show the transmission map as a function of the thicknesses of different layers. In this case, the $\lambda/4$ layers are 124 nm and 160 nm, for SiNx and SiO_2, respectively. The corresponding intensity is designated in the map as $L_{\lambda/4}$. The same shifting behaviour in relation to the coating thicknesses was observed. In this configuration, the higher values of transmission are 99.1% for L_3, 99.9% for $L_{\lambda/4}$, and 99.8% for L_5. ARC of SiNx + SiO_2 have been reported in the literature showing very high

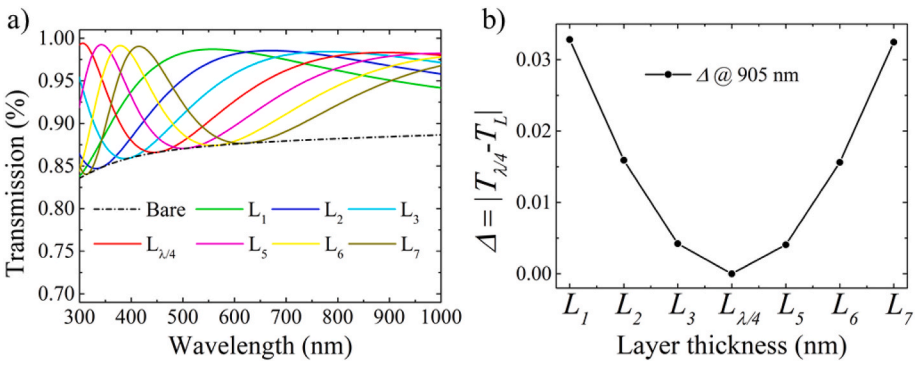

Fig. 6. (a) Transmission spectra for bare PC substrate and with different SiO_2 layers thicknesses. (b) Absolute variation between transmissions at λ_0 nm for $\lambda/4$ layer ($T_{\lambda/4}$) and other layer thicknesses studied (T_L).

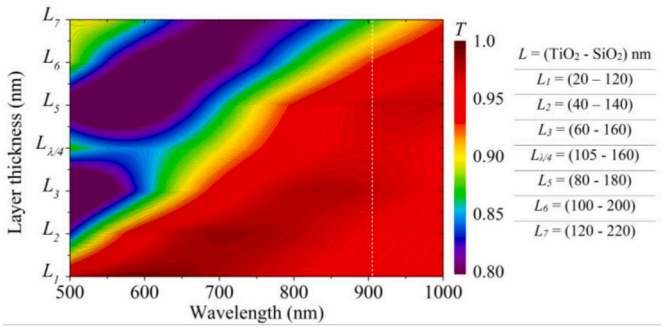

Fig. 7. Transmission intensity map as a function of the thicknesses of the layers for the ARC_2 system. The dashed line is a guide to the eye and marks the λ_0 position on the map.

transmission values. For instance, Zeng et al. [22] reported the observation of 98% of transmission in silicon windows coated on both sides with two periods of SiNx + SiO_2 layers in the wavelength range from 8 μm to 12 μm. Neander et al. [23] have increased the transmission of glass substrate solar cells by applying an ARC formed by two pairs of SiNx + SiO_2 layers on one side of the substrate. The transmission of the uncoated solar cells samples was 90%, being increased to 95% after the coating application in the NIR range of the electromagnetic spectrum.

We also compared the transmission intensity of $\lambda/4$ and the other coating thicknesses considered in the calculations. Fig. 10a shows that an enhancement in the transmission is observed for all the configurations in ARC_3. The thicknesses L_3, and L_5 show comparable transmission values as that for thickness $\lambda/4$, exhibiting an absolute difference Δ close to zero, as can be seen in Fig. 10b.

3.3. Comparison between calculations and experimental measurements using the thin film ARC

After the calculations, we deposited the three ARC on the PC substrates and the experimental transmissions of optical systems were measured. The results obtained are shown in Fig. 11. It is important to note that for the depositions of the films, we considered the thickness L_5 for all the three ARC.

In Fig. 11, we can see that the light transmission is enhanced for all the fabricated ARC systems. The most efficient is the ARC_3 system, exhibiting a measured transmission of 99.1% at λ_0, followed by ARC_1 with 97% of transmission, and ARC_2 with 96% of transmission, in good agreement with the numerical simulations. To further attest this, Fig. 12 compares the experimental and numerical results for each of the ARC systems. In this cases, the calculations were performed taking into

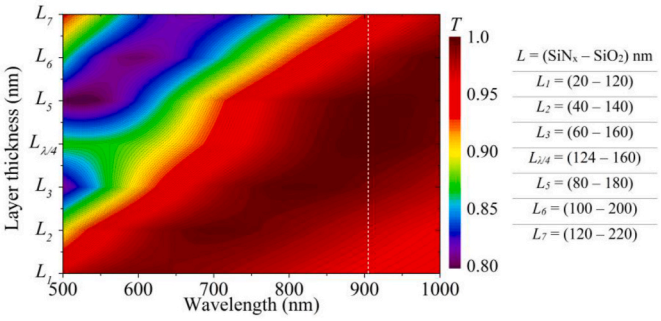

Fig. 9. Transmission intensity map as function of the thicknesses of the layers for the ARC_3 system. The dashed line is a guide to the eye and marks the λ_0 position on the map.

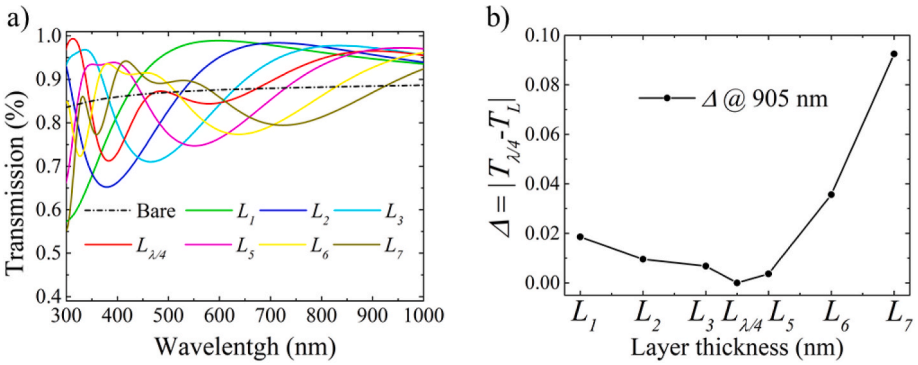

Fig. 8. (a) Transmission spectra for bare PC substrate and for different front and back layer thicknesses. (b) Absolute variation between transmissions at λ_0 for $\lambda/4$($T_{\lambda/4}$) layer and the other layer thicknesses (T_L).

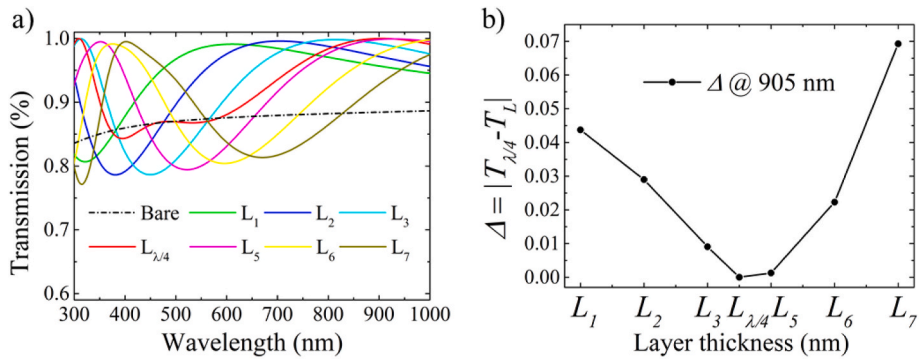

Fig. 10. (a) Transmission spectra for bare PC substrate and for different front and back layer thicknesses. (b) Absolute variation between transmissions at λ_0 for $\lambda/4$ ($T_{\lambda/4}$) layer and the other layer thicknesses (T_L).

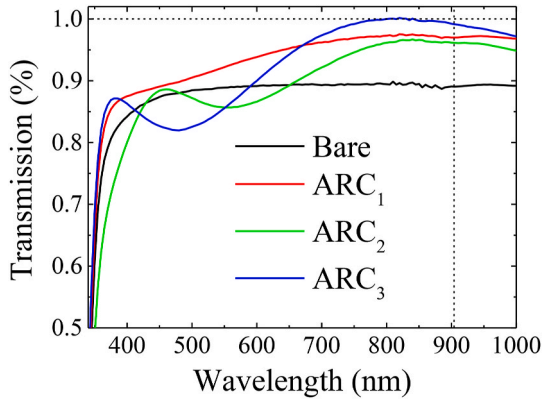

Fig. 11. Transmission spectra obtained for all optical systems studied. The black line represents the transmission of the bare substrate. Red, green, and blue lines represent the transmission spectra for ARC_1, ARC_2, and ARC_3, respectively.

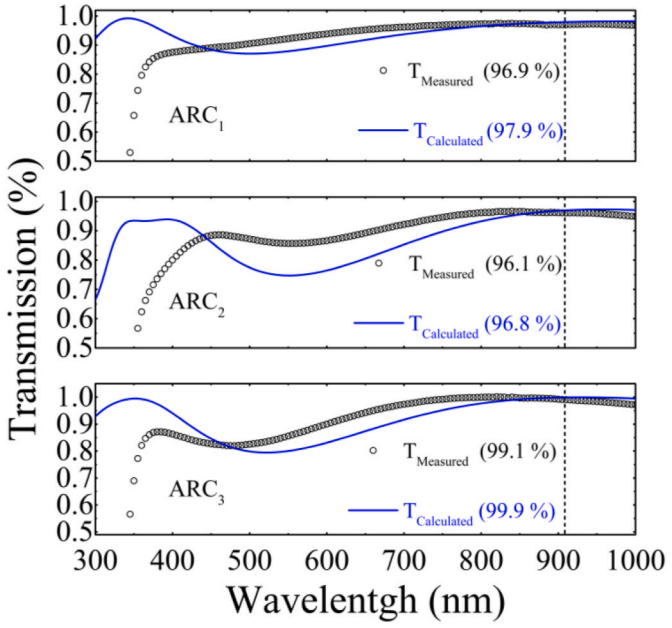

Fig. 12. Comparison between measured and calculated transmissions for the three ARC systems studied. Black symbols represent the measured transmissions (T_{Measured}); the blue lines represent the transmissions calculated ($T_{\text{Calculated}}$) using the average thicknesses. The dashed line represent the wavelength of interest, 905 nm.

account the average thicknesses experimentally measured, namely 180 nm for SiO_2, 80 nm for TiO_2, and 80 nm for SiNx.

Once again, a good agreement was observed between the measured and calculated spectra at the wavelength of interest, as shown in Fig. 12. In particular, at 905 nm the relative difference between the measured and calculated transmission is negligible, being lower than 1%. It is important to highlight that the developed ARC accomplish with one objective of the present work, which relied on keeping the fabrication process simple, once a low number of layers was used to achieve high values of transmission, using deposition techniques that are already available and applied in industry. Furthermore, the ARC describe here are amphiphilic, which in other words, present self-cleaning properties making them interesting to be applied to parts subject to outdoor conditions, such as, lenses of LiDAR systems [4].

3.4. Theoretical comparison between ARC: thin films vs. NP

We also investigated a simple nanostructured system formed by a hexagonal array of circular NP to improve the transmission of the PC substrate. A variety of micro and nanostructures, able to suppress the reflection of light from different substrates, such as glass, polymers, silicon, and others, has been proposed in the literature. These include biomimetic nanostructures, as the moth-eye [24], as well as gratings [25], micro and nano textures [26], and NP [27].

In this study, the array of NP is thought to behave as an ARC with an effective RI (*Neff*), defined by $Neff = \sqrt{n_0\, n_s}$, where $n_0 = 1$ (RI of the air) and $n_s = 1.65$ (RI of the PC) at λ_0. Thus, as a first assumption, the height of the NP array can be defined similarly to the thickness of an thin film ARC by:$H = \lambda_0/4\, Neff$. In addition, to define the parameters a and r, we applied the effective medium approximation, therefore relating the volume fractions (f) of the air and the PC within the unitary cell of the NP array (see inset of Fig. 13a) to the *Neff*:

$$Neff = f.n_s + (1-f).n_0 \tag{1}$$

As f is related to the geometrical parameters of the NP, the relation between a and r is derived as$r = 0.35a$. As a starting point for the geometry of the NP array, among other options, we selected $a = 600$ nm, which renders $r = 210$ nm, and from the first assumption, $H = 175$ nm. In Fig. 13a, we show the resulting transmission of a system with this configuration, at λ_0. As expected, a high transmission of $T = 99.9\%$ was found. In order to better understand the optical behaviour of the current system, variations of H, r, and a were taken around the three values chosen previously. The results are shown in Fig. 13b–d.

Fig. 13b exhibits the transmission response of the system upon the variation of the radius of the NP, keeping constant H and a. In this case, H and a were 175 nm and 600 nm, respectively, and the radius changed from 0 to 350 nm in steps of 25 nm. It can be seen that the highest values of the transmission (≈99.9%) at the wavelength λ_0 are observed within the range of $r = 175$ nm to $r = 250$ nm, approximately.

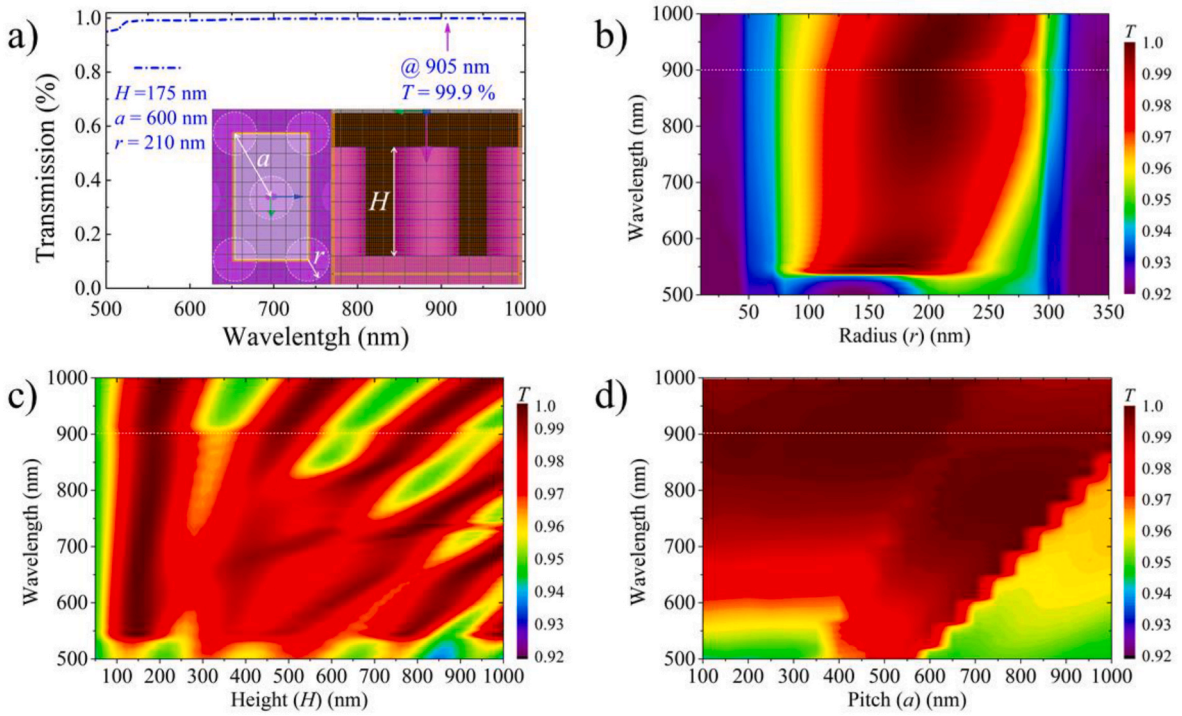

Fig. 13. a) Transmission spectrum obtained with $H = 175$ nm, $r = 210$ nm, $a = 600$ nm as starting parameters. In the insert is the FDTD simulation schematic. Calculated T for: b) Sweep of r. c) Sweep of H. d) Sweep of a. The white line in the maps b, c, and d represents the position of λ_0.

Then, a second sweep was done by fixing the values of r and a, and varying H. In this case, $r = 210$ nm and $a = 600$ nm, respectively. H was varied from 0 to 1000 nm in steps of 50 nm. Fig. 13c shows that at λ_0 the values of $T \approx 99.9\%$ can be observed for 175 nm, 480 nm and 800 nm, within the scanned range.

Lastly, a sweep of the values of a from 100 nm to 1000 nm was performed, in steps of 50 nm, while keeping $H = 175$ nm and $r = 0.35a$, respectively. As can be seen from Fig. 13d the transmission at $\lambda_0$nm is enhanced to $T \approx 99.9\%$ for different combinations of r and a.

A direct comparison between these results when using the NP and the best result obtained using the thin films ARC_3, demonstrates that the highest transmission values found for both approaches are very similar. For the ARC_3, we found that $T_{\lambda/4} = 99.9\%$ (calculation) and $T_{\lambda/4} = 99.1\%$ (measurement), and when NP are used, a transmission value of $T = 99.9\%$ was calculated ($H = 175$ nm, $r = 210$ nm, and $a = 600$ nm, for instance). In addition, if we take into consideration that a manufacture scalable process is essential, and since comparable results were obtained from both approaches, then it is important to highlight that the fabrication of the NP on the surface of the polymeric substrate is much more complex and consequently makes the solution composed of thin films much more attractive for the production of ARC.

4. Conclusions

This study aimed to enhance the transmission of a polymeric substrate using ARC, either formed by the deposition and combination of thin layers of SiO_2, TiO_2, and SiNx, as well as nanostructures on the surface. The ARC were calculated to work at the initial NIR part of the electromagnetic spectrum, with 905 nm as the central wavelength. Since the experimental techniques employed for the deposition of the thin films are compatible and scalable to industry, the investigated ARC are intended to be used in the manufacturing processes of optical lenses for LiDAR systems. In this sense, we investigated numerically and experimentally the transmission of the ARC considering thicknesses different from the theoretical $\lambda/4$ value. The numerical results revealed that these systems present good tolerance to variations of the thickness, with calculated transmissions above 99%, even when the thicknesses of the layers varied by 12%. Additionally, we compared the results obtained with those for a system formed by a hexagonal array of NP and observed that the optimized transmission intensity achieved with these nanostructures is similar that found for the thin film ARC. Furthermore, the experimental results are in good agreement with numerical predictions, demonstrating transmission values as high as 99%. WCA and OCA measurements revealed that the surface wettability of the polymer substrate becomes superamphiphilic after the depositions of the ARC, rendering to the studied systems possible self-cleaning properties.

CRediT authorship contribution statement

P.T. Valentim: Validation, Formal analysis, Software, Investigation, Writing – original draft, Writing – review & editing. **A. Retolaza:** Formal analysis, Investigation, Writing – original draft, Writing – review & editing. **J. Llobet:** Conceptualization, Investigation. **C. Araújo:** Investigation. **S. Cruz:** Investigation. **C. Machado:** Investigation. **A.J.V. Pontes:** Conceptualization, Funding acquisition. **H. Santos:** Conceptualization, Funding acquisition. **P.C. Sousa:** Conceptualization, Methodology, Supervision, Writing – original draft, Writing – review & editing.

Declaration of competing interest

The authors declare that they have no known competing financial interests or personal relationships that could have appeared to influence the work reported in this paper.

Data availability

Data will be made available on request.

Acknowledgments

This work was supported by European Regional Development Fund

(ERDF), through the Competitiveness and Internationalization Operational Program (COMPETE 2020) of the Portugal 2020 Program [SMART4CAR- Smart Surfaces for Automotive Components – POCI - 01-0247-FEDER- 045096]. The authors would like to thank H. Fonseca for his support.

References

[1] P. Colombo, G. Franchin, Printing glass in the nano, Nat. Mater. 20 (2021) 1454–1456.
[2] A. Piegari, F. Flory, Optical Thin Films and Coatings: from Materials to Applications, Woodhead Publishing Limited, Cambridge, UK, 2013.
[3] J. Cai, L. Qi, Recent advances in antireflective surfaces based on nanostructure arrays, Mater. Horiz. 2 (2015) 37–53.
[4] J. Rombaut, S. Martínez, U.M. Matera, P. Mazumder, V. Pruneri, Antireflective multilayer surface with self-cleaning subwavelength structures, ACS Photonics 8 (2021) 894–900.
[5] P. Buskens, M. Burghoorn, M.C.D. Mourad, Z. Vroon, Antireflective coatings for glass and transparent polymers, Langmuir 32 (2016) 6781–6793.
[6] H.K. Raut, V.A. Ganesh, A.S. Nair, S. Ramakrishna, Anti-reflective coatings: a critical, in-depth review, Energy Environ. Sci. 4 (2011) 3779–3804.
[7] S.B. Khan, H. Wu, X. Huai, S. Zou, Y. Liu, Z. Zhang, Mechanically robust antireflective coatings, Nano Res. 11 (2018) 1699–1713.
[8] U. Schulz, Review of modern techniques to generate antireflective properties on thermoplastic polymers, Appl. Opt. 45 (2006) 1608–1618.
[9] C. Garlisi, E. Trepci, X. Li, R. Al Sakkaf, K. Al-Ali, R.P. Nogueira, L. Zheng, E. Azar, G. Palmisano, Multilayer thin film structures for multifunctional glass: self-cleaning, antireflective and energy-saving properties, Appl. Energy 264 (2020), 114697.
[10] B.M. Phillips, P. Jiang, Biomimetic antireflection surfaces, in: Engineered Biomimicry, Elsevier Inc. Chapters, 2013, pp. 305–331.
[11] Z. Pan, F. Cheng, B. Zhao, Bio-inspired polymeric structures with special wettability and their applications: an overview, Polymers 9 (2017) 725.
[12] S. Larouche, L. Martinu, OpenFilters: open-source software for the design, optimization, and synthesis of optical filters, Appl. Opt. 47 (2008) C219–C230.
[13] S. Nundy, A. Ghosh, T.K. Mallick, Hydrophilic and superhydrophilic self-cleaning coatings by morphologically varying ZnO microstructures for photovoltaic and glazing applications, ACS Omega 5 (2020) 1033–1039.
[14] X. Li, J. Yang, J. Wanga, X. Chang, J. Xu, Z. Wud, A stable super-amphiphilic surface created from superhydrophobic silica/epoxy coating by low-temperature plasma-treatment, Surf. Eng. 37 (2015) 1282–1289.
[15] S. Olveira, A. Stojanovic, S. Seeger, Superhydrophilic and superamphiphilic coatings, in: L. Wu, J. Baghdachi (Eds.), Functional Polymer Coatings: Principles, Methods, and Applications, John Wiley & Sons, Inc, Hoboken, NJ, 2015, pp. 96–132.
[16] R. Wang, K. Hashimoto, A. Fujishima, M. Chikuni, E. Kojima, A. Kitamura, Light-induced amphiphilic surfaces, Nature 388 (1997) 431–432.
[17] P. Chen, Y. Hu, C. Wei, Preparation of superhydrophilic mesoporous SiO_2 thin films, Appl. Surf. Sci. 258 (2012) 4334–4338.
[18] H. Sayed, Z.S. Matar, M. Al-Dossari, A.F. Amin, N.S.A. El-Gawaad, A.H. Aly, The design and optimization of an anti-reflection coating and an intermediate reflective layer to enhance tandem solar cell photons capture, Crystals 12 (2021) 57.
[19] H.M. Yadav, J.-S. Kim, Fabrication of SiO2/TiO2 double layer thin films with self-cleaning and photocatalytic properties, J. Mater. Sci. Mater. Electron. 27 (2016) 10082–10088.
[20] Y. Matsuoka, S. Mathonnèire, S. Peters, W.T. Masselink, Broadband multilayer anti-reflection coating for mid-infrared range from 7 μm to 12 μm, Appl. Opt. 57 (2018) 1645–1649.
[21] D.F. Zambrano, R. Villarroel, R. Espinoza-González, N. Carvajal, A. Rosenkranz, A. G. Montaño-Figueroa, M.J. Arellano-Jiménez, M. Quevedo-Lopez, P. Valenzuela, W. Gacitúa, Mechanical and microstructural properties of broadband anti-reflective TiO_2/SiO_2 coatings for photovoltaic applications fabricated by magnetron sputtering, Sol. Energy Mater. Sol. Cell. 220 (2021), 110841.
[22] Hong-Yuan Zeng, Shiang-Feng Tang, Tzu-Chiang Chen, Performance evaluation for uncooled microbolometer using antireflection coating of SiO_2/Si_3N_4 multiple films on silicon window, Sensor. Mater. 30 (2018) 339–345.
[23] M. Neander, F. Gromball, D. Neumann, N. Harder, W. Nositschka, Anti-reflective-coating tuned for higher solar module voltage, in: 2006 IEEE 4th World Conference on Photovoltaic Energy Conference, 2006, pp. 2070–2072.
[24] H. Xu, L. Gong, S. Zhang, R. Ma, L. Pen, J. Zhao, Y. Li, Biomimetic moth-eye anti-reflective poly-(methyl methacrylate) nanostructural coating, JBE 16 (2019) 1030–1038.
[25] Y. Kanamori, M. Okochi, K. Hane, Fabrication of antireflection subwavelentgh gratings at the tips of optical fibers using UV nanoimprint lithography, Opt Express 21 (2013) 322–328.
[26] Y. Nishijima, R. Komatsu, S. Ota, G. Seniutinas, A. Balčytis, S. Juodkazis, Anti-reflective surfaces: cascading nano/microstructuring, APL Photonics 1 (2016), 076104.
[27] S. Dong, J. Zhang, H. Jiao, W. Zhang, X. Li, Z. Wang, X. Cheng, Nanopillars assisted multilayer antireflection coating for photovoltaics with multiple bandgaps, Appl. Phys. Lett. 115 (2019), 133106.